

Article

X-ray Photoelectron Spectroscopy Analysis of Nitrogen-Doped TiO₂ Films Prepared by Reactive-Ion-Beam Sputtering with Various NH₃/O₂ Gas Mixture Ratios

Jin-Cherng Hsu ^{1,2,*}, Yung-Hsin Lin ² and Paul W. Wang ³

¹ Department of Physics, Fu Jen Catholic University, No.510 Zhongzheng Rd., Xinzhuang Dist., New Taipei City 24205, Taiwan

² Graduate Institute of Applied Science and Engineering, Fu Jen Catholic University, No. 510 Zhongzheng Rd., Xinzhuang Dist., New Taipei City 24205, Taiwan; stanley290@yahoo.com.tw

³ Department of Physics, Bradley University, Peoria, IL 61606, USA; pwang@bradley.edu

* Correspondence: 054326@mail.fju.edu.tw; Tel.: +88-62-2905-3765; Fax: +88-62-2902-1038

Received: 4 December 2019; Accepted: 2 January 2020; Published: 4 January 2020



Abstract: Nitrogen-doped TiO₂ films were prepared by reactive ion-beam sputtering deposition (IBSD) in a mixed atmosphere of NH₃ and O₂ at a substrate temperature of 400 °C. X-ray photoelectron spectra revealed the presence of six ions, i.e., N³⁻, N²⁻, N¹⁻, N⁺, N²⁺, and N³⁺, respectively, in the films. The amorphous films had complex, randomly oriented chemical bonds. The Tauc–Lorentz model was employed to determine the bandgap energy of the amorphous films prepared using different NH₃/O₂ gas mixing ratios by ellipsometry. In addition, the optical constants of the films were measured. With the increase in the NH₃/O₂ gas mixture ratio to 3.0, the bandgap of N-doped TiO₂ narrowed to ~2.54 eV.

Keywords: nitrogen-doped TiO₂; Tauc–Lorentz model; NH₃/O₂ gas mixture; bandgap narrowing

1. Introduction

TiO₂ films doped with metal and non-metal species are extremely interesting materials due to their potential for use in heterogeneous photocatalysis. Among all nonmetal-doped TiO₂ materials, N-doped TiO₂ is the most investigated material due to the fact that its nanomaterials exhibit superior photocatalytic activity with respect to pure TiO₂ due to band-gap narrowing under visible-light irradiation. There are three major views with respect to the modification mechanism of N-doped TiO₂, namely, bandgap narrowing, impurity energy level, and oxygen vacancies [1]. The N_{2p} state undergoes hybridization with the O_{2p} states in N-doped TiO₂ due to their similar energies. Thus, the narrow bandgap can absorb visible light [2]. As N atoms replace O sites of TiO₂, isolated impurity levels above the valence band (VB) are formed as shallow acceptor states, with visible-light illumination leading to electron excitation [3,4]. Oxygen-deficient sites that form in the grain boundaries of N-doped TiO₂ films are key to the emerging visible-light activity. The N-doped part of an oxygen-deficient site is crucial to block reoxidation [5].

Kusano et al. concluded that N atoms were incorporated into TiO₂ lattices as interstitial nitrogen (N_i) and substitutional nitrogen (N_s) [6]. Density functional theory revealed that N preferred to replace Ti atoms rather than O atoms [7]. Asahi et al. made a theoretical comparison between N_s, N_i, and both types of dopants in the anatase TiO₂. The dopants give rise to the bonding states below the O_{2p} valence bands and antibonding states deep in the bandgap. However, these states were well screened and hardly interacted with the band states of TiO₂ [2]. They also emphasized the importance

of substitutional site N doping and clearly observed an increase of photocatalytic activity by increasing the component of N, with an X-ray photoelectron spectroscopy (XPS) peak at 396 eV. Although several theoretical and experimental studies have been conducted on N-doped TiO₂, some issues, such as the photocatalytic activity origin of structural defects under visible light and the chemical and electronic states of the constituent elements (Ti, O, N), are still worthy of further study. Generally, photocatalytic activity and chemical and electronic states were investigated by UV-visible absorption experiments and X-ray photoelectron spectroscopy (XPS) analysis, respectively. N-doped TiO₂ can be prepared by physical or chemical methods, such as the sol-gel method [6], microwave plasma synthesis [8], sputtering [9], laser pyrolysis [10], plasma-enhanced chemical vapor deposition [11], hydrothermal processing [12], or annealing of TiO₂ films in gaseous NH₃ [13]. In this study, N-doped TiO₂ films were fabricated using different NH₃/O₂ gas mixture ratios with reactive ion-beam sputtering deposition (IBSD) to achieve nitridization or oxidation of the film at a high substrate temperature of 400 °C under high vacuum conditions of $\sim 10^{-4}$ Torr. During the process, the above-mentioned debate was expected to be solved via the reaction control of pure titanium atoms generated by ion-beam sputtering with the nitrogen atoms produced by the ionization of the NH₃ ambient gas due to its low bond energy of 3.5 eV [14].

2. Materials and Methods

Figure 1 shows a schematic representation of the experimental procedure.

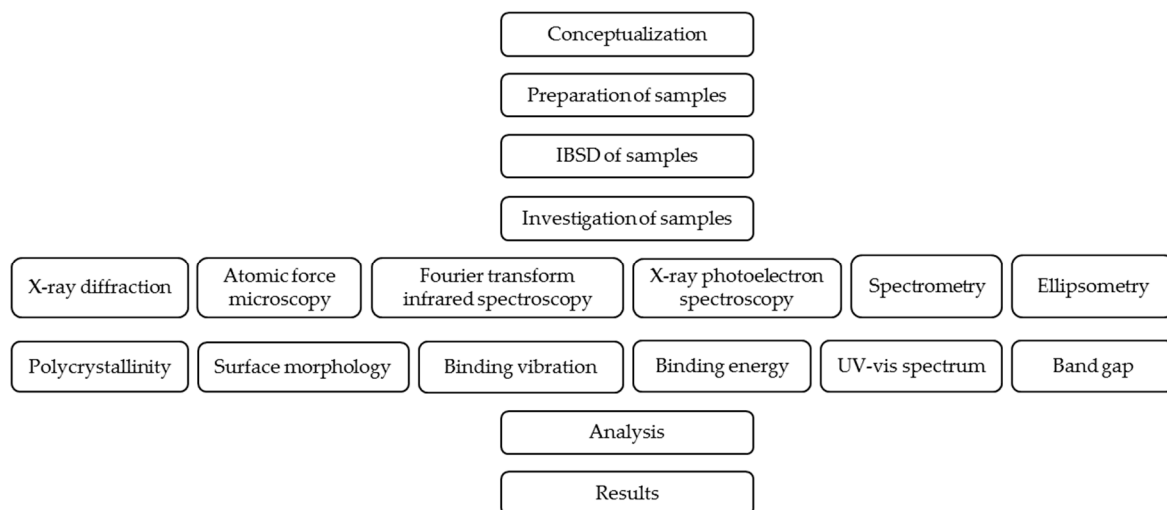


Figure 1. Schematic representation of the experimental procedure.

2.1. Preparation of Coated Surfaces

Optical properties and compositions of titanium oxynitride films prepared by IBSD were investigated. IBSD technology exhibits characteristics of a stable deposition speed, low pollution, and precise composition control [15]. Titanium oxynitride films were deposited onto fused silica substrates at a substrate temperature of 400 °C via sputtering of a metal titanium target (99.99% purity) mounted on a water-cooled copper block at an angle of 45° in the ion-beam direction. A homemade vacuum chamber with a diameter of 40 cm was evacuated using a cryogenic pump at a base pressure of less than 5×10^{-6} Torr and was arranged in a 3-cm Kaufman ion source with a mass-flow meter to supply Ar working gas. NH₃ and O₂ gases were fed into the chamber by controlling mass-flow meters. The total pressure was 2×10^{-4} Torr during the deposition. An energetic ion beam at a voltage of 1000 V and a current of 30 mA cleared the titanium target surface for 15 min before deposition. When opening the substrate shutter, the films were deposited at a rate of 0.02–0.03 nm/s, and their thicknesses were controlled at ~ 400 nm by using a quartz crystal monitor. During the deposition, the partial NH₃ pressure was controlled at 0.5×10^{-4} , 0.75×10^{-4} , 1.0×10^{-4} , and 1.5×10^{-4} Torr. Then, oxygen gas was

simultaneously supplied at NH₃ to O₂ partial pressure ratios of 0.5, 1, 2, and 3, and the as-deposited films were labeled as TiON-0.5, TiON-1, TiON-2, and TiON-3, respectively.

2.2. Investigation of Samples

Crystalline structures of the films were examined using an X-ray diffractometer (Multiflex, Rigaku Corporation, Tokyo, Japan) with a copper K_α line at 1.54055 Å. The film morphology was monitored using a Dimension 3100 atomic force microscope (Veeco Instruments Inc., New York, NY, USA). XPS profiles of the films were recorded on a Kratos Axis Ultra DLD spectrometer (Warwick Photoemission Facility, West Midlands, UK). Film transmittance was examined on a Varian Cary 5E spectrometer (Varian, CA, USA) at wavelengths of 200–1000 nm in the visible spectrum. Other optical properties, such as the refractive index (*n*) and extinction coefficient (*k*), were measured using an ellipsometer, VASE M44 (J. A. Woollam Co., Inc., Lincoln, NE, USA). The front surfaces of the samples were irradiated by polarization light at four incident angles of 60°, 65°, 70°, and 75°, respectively. The Ψ and Δ values of the films deposited on fused silica substrates in an optical wavelength range from 350–1000 nm were obtained by ellipsometry, which was performed with a focused beam. A model other than the Tauc–Lorentz model was used to fit the ellipsometry data, therefore, it was difficult to determine the bandgap energy caused by the optical absorption of the intraband or defects in the composite amorphous film [16–18]. The model expressed the imaginary part of the dielectric function ε₂ (= 2*nk*) at a photon energy *E* as follows:

$$\varepsilon_2 = \frac{A(E - E_g)^2 CE_0}{(E^2 - E_0^2)^2 + C^2 E^2}, \text{ as } E > E_g \quad (1)$$

$$\varepsilon_2 = 0, \text{ as } E \leq E_g \quad (2)$$

where four parameters are comprised: The prefactor *A* (the amplitude of the oscillator), the bandgap energy *E_g*, the broadening parameter *C*, and the peak in the joint density of states *E₀*. This four-parameter model is typically sufficient to describe the optical functions of the amorphous film by the ellipsometry software of VASE M44 [19].

In this study, the Tauc–Lorentz model was utilized to fit the measured Ψ and Δ values for the four incident angles. The mean squared error (MSE) is a measure of the quality of an estimator, i.e.,

$$\text{MSE} = \frac{1}{2N - M} \sum_{i=1}^N \left[\left(\frac{\Psi_i^{\text{mod}} - \Psi_i^{\text{exp}}}{\sigma_{\Psi_i}^{\text{exp}}} \right)^2 + \left(\frac{\Delta_i^{\text{mod}} - \Delta_i^{\text{exp}}}{\sigma_{\Delta_i}^{\text{exp}}} \right)^2 \right] \quad (3)$$

where *i* = 1 to *N*; Ψ^{exp} and Δ^{exp} represent the experimental data and Ψ^{mod} and Δ^{mod} represent the fitting data, respectively. *N* and *M* represent the number of the measured Ψ–Δ pairs and the fitting parameters, respectively and σ_Ψ^{exp} and σ_Δ^{exp} represent the standard deviations of Ψ and Δ experimental data points, respectively. In the equation, the prefactor comprises 2*N* due to the inclusion of the two measured values in the calculation for each Ψ–Δ pair [19]. Figure 2 shows a fitting example of the TiON-3 film expressed by Ψ and Δ. The MSE values of the samples were less than 5.

Fourier transform infrared (FTIR) spectroscopy (PE-2000-type PerkinElmer, Waltham, MA, USA) was employed to investigate the hydrogen, hydroxyl, and NH₃ bonds in the films. XPS (Axis Ultra DLD system, Kratos Analytical Ltd., Manchester, UK) was employed to examine the chemical bonds and atomic concentrations of the films, which were etched for 30 s before measurement. Binding energies (BEs) of the components obtained from the fitting program applied to the Ti_{2p}, O_{1s}, and N_{1s} XPS spectra were utilized to deduce the oxidation states and chemical bonding environments of the atoms in the films.

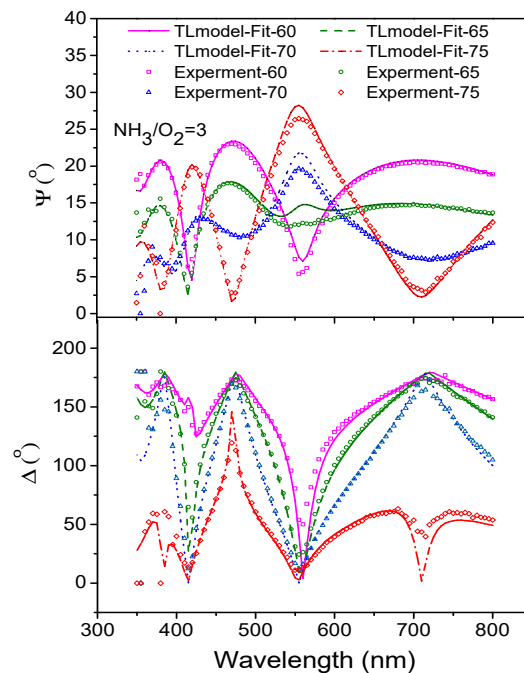


Figure 2. A fitting example of the TiON-3 film expressed by Ψ and Δ with a root mean square (RMS) of 4.8.

3. Results and Discussion

3.1. XRD of N-Doped TiO_2 Films

Generally, the titanium dioxide film deposited at a substrate temperature of 400 °C exhibited an anatase structure, with a sharp (101) peak observed at $2\theta = 25^\circ$ in the XRD spectrum [20,21]. Karunagaran et al. also found that the structures of the films deposited at ambient temperature were amorphous, whereas the films annealed at 400 °C and above were crystalline with anatase [22]. However, doped titanium oxide co-sputtered with a metallic aluminum target or a semiconductor silicon target led to reduced polycrystallinity in the structure [23,24]. In this study, the titanium dioxide film was doped with nitride by IBSD under different NH_3/O_2 gas mixtures. The argon ion beam bombarded the metallic titanium target, and the sputtered titanium atoms exhibited more energy to react with the NH_3 and O_2 gases on the target surface [21]. Equipped with the kinetic energy of several electron volts, the reaction atoms that accumulated on the fused silica substrate surface [25], where the substrate temperature was 400 °C, enhanced the formation of the deposited titanium oxynitride species. However, although these films were deposited at high substrate temperatures under an NH_3/O_2 gas mixture ratio of ≥ 0.5 , the XRD spectra indicated that the films were not anatase, but rather amorphous, due to the change in the lattice parameters, bond length, and charges on the Ti atom caused by the complex dopant N ions [4].

3.2. Surface Morphology of N-Doped TiO_2 Films

The surface morphology of amorphous films revealed that the surface roughness was less than that of a pure polycrystalline film [21]. The NH_3/O_2 gas mixture ratio affected the surface roughness of the film prepared by IBSD. For example, the root mean square (RMS) roughness of the TiON-2 sample was 0.187 nm, a value that was about four times less than TiON-0.5, which was 0.651 nm (Figure 3). Moreover, the atomic radius of the nitrogen atom was greater than that of the oxygen atom. When N atoms were substituted for O atoms in the TiO_2 film, the bond length, lattice constant, and atomic volume all changed, leading to the weak anisotropy of anatase. The N-dopants randomly bonded to titanium dioxide in the film, as observed by the XRD inhibition. In the pitch multiplication process for

integrated circuit fabrication, the amorphous titanium oxynitride film was capable of depositing a thick, smooth, and amorphous film to form spacers [26].

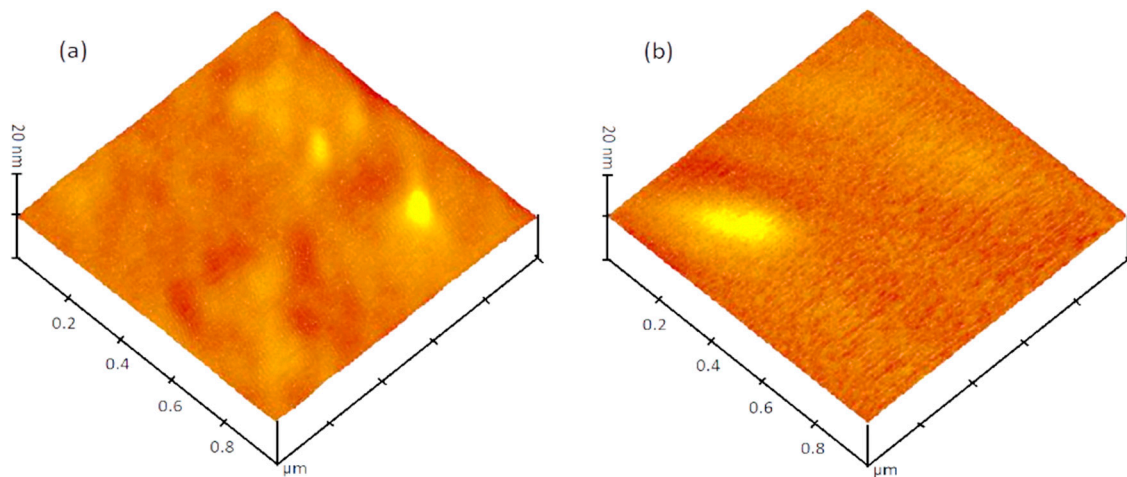


Figure 3. (a) Surface morphology of TiON-0.5 with a surface roughness (RMS) of 0.7 ± 0.1 nm. (b) Surface morphology of TiON-2 with a surface roughness (RMS) of 0.2 ± 0.1 nm.

3.3. FTIR Spectra of N-Doped TiO₂ Films

Vietro et al. examined the dissociation of the NH₃/O₂ gas mixture by radio-frequency (RF) glow discharge. NH₃ gas feed produced H atoms, NH radicals, and excited N₂; and O₂ gas feeds produced O atoms and excited O₂ [27]. Therefore, the plasma contained OH radicals, H₂O, and NO_x species in the IBSD process. Species of NH₃ and H₂O molecules in the plasma that did not react with the sputtered titanium atoms might have been present in the film, even though the molecules were continuously pumped out of the chamber under high vacuum conditions. Figure 4 shows the FTIR spectra of the films, which were recorded under various NH₃/O₂ gas mixing ratios.

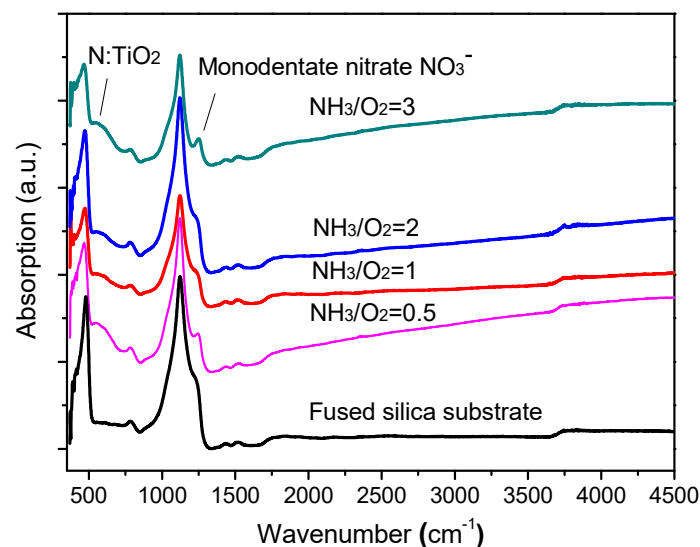


Figure 4. Fourier transform infrared (FTIR) spectra of N-doped TiO₂ films.

Characteristics of anatase and rutile corresponding to the Ti–O stretching vibrations [28] were absent in the range from 440 to ~ 505 cm^{−1} in their FTIR spectra compared with that of the fused silica substrate. Hence, the as-deposited films were amorphous, as mentioned in Section 3.1. The small peak observed at 800 cm^{−1} corresponded to the Si–O–Si bending vibration. The peak at 950 cm^{−1} (O-doped amorphous silicon) to 1075 cm^{−1} (stoichiometric SiO₂) corresponded to the SiO_x stretching

vibration ($0 < x < 2$) in the FTIR spectrum of the fused silica substrate. With the decrease in the oxygen concentration, the broad shoulder extended to a high frequency of 1300 cm^{-1} and merged with the main band [29]. Small peaks were observed at ~ 1460 , 1514 , and 1735 cm^{-1} , which were characteristic of C–H, C=C, and C=O bonds of the contaminant, respectively [30,31]. NH_3 (1225 , 3154 , 3195 , 3255 , and 3393 cm^{-1}) [32], nitrogen-related hydrogen bonds (at 1150 – 1220 , 1300 – 1350 , 1560 – 1610 , and 3150 – 3393 cm^{-1}) and hydroxyl radical bonds (3200 – 3400 cm^{-1}) [33] completely disappeared from the FTIR spectra when the substrate temperature was $400\text{ }^\circ\text{C}$ during the deposition. The FTIR spectra of the films prepared using various gas ratios were similar to that of the fused silica substrate, except for a low-intensity broad peak at 620 cm^{-1} for the N-doped TiO_2 [28] and a small peak at 1250 cm^{-1} for the monodentate nitrate [34]. The absorber NO species of the film that were deposited using different NH_3/O_2 gas mixture ratios are discussed in the following section.

3.4. X-ray Photoelectron Spectra of N-Doped TiO_2 Films

The XRD inhibition of the N-doped TiO_2 film exhibited a change in the chemical bonds of the film. XPS is one of the most suitable techniques to directly observe the N-derived state from the photoelectron BE.

3.4.1. O_{1s} XPS Spectra

Figure 5 shows the O_{1s} XPS spectra of the N-doped TiO_2 films fabricated under various NH_3/O_2 gas mixing ratios. All of the films exhibited amorphous structures, as mentioned in Section 3.1. Typically, the XPS peaks corresponding to core-level electrons were broad due to the less-localized electron density distribution [35]. The XPS spectra with shoulders were decomposed into two peaks, i.e., bridging oxygen (BO) and high-binding-energy oxygen (HBO). The main peak at 530.1 eV with the largest area corresponded to BO, where the O atom was the dominant species in the Ti–O linkage.

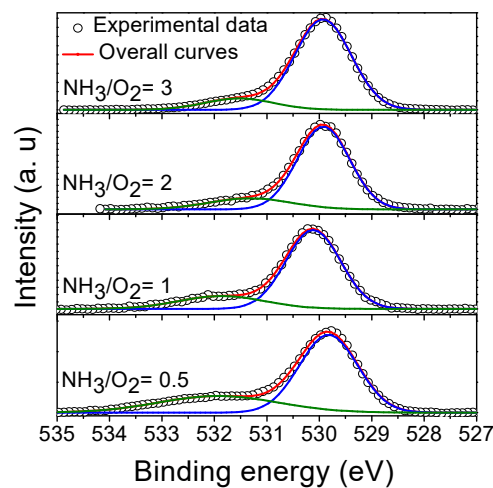


Figure 5. O_{1s} XPS spectra of the films fabricated under various gas ratios.

The HBO sub-peak at a higher BE energy of 531.5 – 532 eV resulted from a lack of electrons in the non-stoichiometric oxygen atom, which corresponded to oxygen in the Ti–O–N or Ti–N–O bonds [36–38]. With the increase in the NH_3/O_2 gas ratio, the peak area and BE decreased, resulting from the increase in the number of electrons provided by the nitrogen atoms. Compared with our previous results regarding co-sputtering of a Ti target with an Al or Si target [22,23], the HBO area of N-doped TiO_2 decreased with the increase in the doping material, which was contrary to the increase in HBO areas of Al-doped or Si-doped TiO_2 , also indicating that nitrogen-dopants provided more electrons to oxygen atoms than the Al and Si dopants during the IBSD process. The oxidation states of the N atoms in N-doped films fabricated by IBSD using different NH_3/O_2 gas mixtures are discussed again in Section 3.4.3.

3.4.2. X-ray Photoelectron Spectroscopy of Ti

The Ti XPS signal comprised two peaks, i.e., weak $Ti2p_{1/2}$ and strong $Ti2p_{3/2}$ (Figure 6). Previous studies reported that each peak was decomposed into three sub-peaks, with components of Ti^{4+} , Ti^{3+} , and Ti^{2+} , respectively: Ti^{4+} ($2p_{1/2}$ at ~ 464.5 eV, $2p_{3/2}$ at ~ 458.9 eV), Ti^{3+} ($2p_{1/2}$ at ~ 462.8 eV, $2p_{3/2}$ at ~ 457.3 eV), and Ti^{2+} ($2p_{1/2}$ at ~ 460.9 eV, $2p_{3/2}$ at ~ 455.6 eV) [23,39]. In this study, however, the $Ti2p_{1/2}$ and $Ti2p_{3/2}$ XPS peaks were mainly located at 464.2 and 458.5 eV, respectively. With the change in the NH_3/O_2 gas mixture ratio, their areas exhibited marginal changes and were composed of lower-energy peaks of Ti^{3+} and Ti^{2+} , as reported by Jia et al. for N-doped TiO_2 nanocrystals [40].

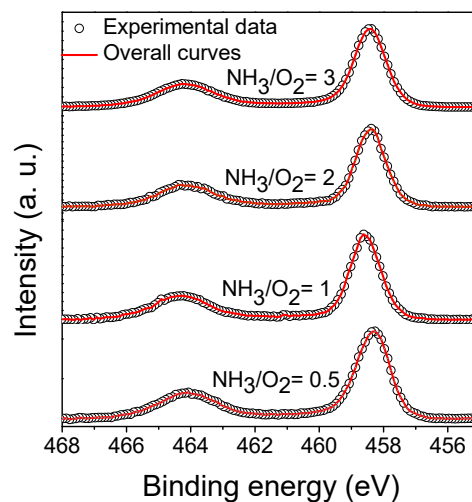


Figure 6. Ti_{2p} XPS spectra of the films fabricated under various gas ratios.

Compared with our previous study involving the co-sputtering of Al or Si, the increases in the amounts of Ti^{3+} and Ti^{2+} in the N-doped film were less than those of the Al-doped or Si-doped TiO_2 films [22,23]. Moreover, the electronegativity of the nitrogen atom (3.06) was similar to that of the oxygen atom (3.44). That is, the high electronegativity of the nitrogen atom led to the complete oxidation of the titanium atom in the N-doped TiO_2 film. Hence, Ti^{4+} peaks were mainly observed in the XPS spectra of the N-doped TiO_2 films. Yu et al. also explained that some Ti^{2+} reacted with N^{1-} to form Ti^{3+} , followed by a reaction with N^{1-} or N^{2-} to form Ti^{4+} . Therefore, only Ti^{4+} was present in all of the films deposited using various NH_3/O_2 gas mixing ratios [36].

3.4.3. XPS of N

The XPS N_{1s} spectra exhibited six fitted sub-peaks (Figure 7). The six sub-peaks were located at average BEs of 395.93, 396.92, 397.84, 399.55, 400.58, and 401.68 eV, corresponding to the oxidation states of N^{3-} , N^{2-} , N^{1-} , N^{1+} , N^{2+} , and N^{3+} species, respectively (Table 1).

Table 1 summarizes the full width at half maximum (FWHM), BE, and the difference (Δ) between adjacent oxidation states of the six sub-peaks. The Δ values fluctuated by ~ 1 eV due to the complex nitrogen bonding. The N^0 oxidation state is not listed in Table 1 due to the absence of the N^0 bond from the films, which was caused by electrical neutralization. Table 2 summarizes the BEs and types of bonds in the six N oxidation states of N^{3-} to N^{3+} . The N^{3-} species at the lowest average BE of 395.9 eV substituted the O^{2-} site in TiO_2 and formed the N–Ti chemical bond [2,36,41]. With the increase in the NH_3/O_2 gas mixing ratio, the relative concentration of the N^{3-} species clearly increased, while those of the N^{1-} and N^{2-} species decreased (Figure 7). The BE of the N^{3-} slightly increased and the FWHM decreased (Table 1) due to the purification of the N^{3-} species. Hence, N–Ti bonds were formed at high NH_3/O_2 gas mixing ratios. However, the optical absorption increased as the form of the N–Ti bonds changed in the optical spectrum, as explained in Section 3.5.

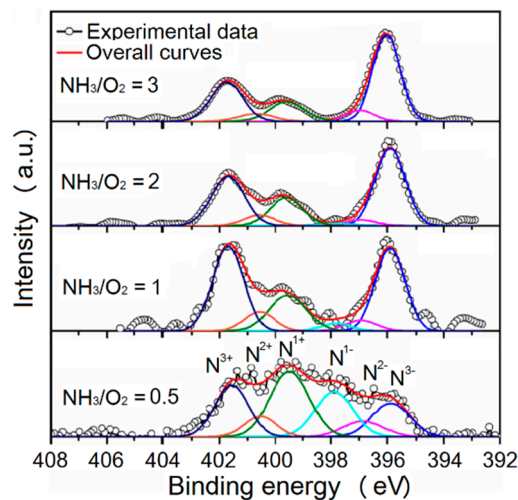


Figure 7. Original and fitted N1s XPS spectra of titanium oxynitride films prepared using different NH_3/O_2 ratios. Six components of N^{3-} , N^{2-} , N^{1-} , N^{1+} , N^{2+} , and N^{3+} , respectively, from low to high binding energy (BE), were applied to spectral fitting.

Table 1. Summary of all of the components of N_{1s} in titanium oxynitride films.

Oxidation States		N^{3+}	N^{2+}	N^{1+}	N^{1-}	N^{2-}	N^{3-}
TiON-0.5	BE	401.6	400.5	399.5	397.9	396.9	395.9
	Δ *	–	1.0	1.1	–	1.1	1.0
	FWHM	0.60	0.6	0.7	–	0.7	0.7
TiON-1	BE	401.7	400.6	399.6	397.8	396.9	395.9
	Δ	–	1.1	1.0	–	0.9	1.0
	FWHM	0.6	0.6	0.7	0.5	0.6	0.5
TiON-2	BE	401.7	400.6	399.6	397.8	396.9	395.9
	Δ	–	1.1	1.0	–	0.9	1.0
	FWHM	0.6	0.6	0.6	0.6	0.5	0.5
TiON-3	BE	401.7	400.7	399.6	–	397.0	396.0
	Δ	–	1.0	1.1	–	–	0.9
	FWHM	0.6	0.6	0.6	–	0.5	0.5
Average of BE		401.7	400.6	399.6	397.8	396.9	395.9

* Δ : BE difference between adjacent oxidation states; Unit: eV. Error = 0.5 eV.

Table 2. Binding energies and types of bonding in the six N oxidation states.

Oxidation States	Binding Energy (eV)	Bonding	Reference
N^{3-}	396	N–Ti, N–Ti–O	[2,36,41]
N^{2-}	395.4, 395.7, 396, 396.3, 396.6, 396.9, 397.2, 397.5	Ti–N–Ti–O, Ti–N–Ti–N, O–Ti–N (N^{3-} substitute O^{2-})	[36–50]
N^{1-} , N^{1+}	398.7, 398.2, 399, 399.1	N–O, N–Ti–O, $\text{N}\equiv\text{O}$ (in TiO_xN_y)	[37,39,41,42,46,47,50]
N^{2+} , N^{3+}	399.8, 400, 400.2, 401.8, 402	Ti–O–N–O	[41,43,44,47]

As summarized in Table 1, the average next lower BE for the N^{2-} species was 396.92 eV due to the decrease in the number of electrons surrounding the N ions, which was formed by Ti–N–Ti–O or Ti–N–Ti–N bonds due to the chemical absorption of nitrogen on the surface or complex bonding of oxynitride (Table 2). The Ti atom was bonded to not only the N atoms but also another atom, leading to an increase in the BE of N^{2-} compared with N^{3-} . With the increase in the gas mixture ratio, the BE increased and the FWHM decreased, similar to the trend observed for the N^{3-} species.

When the oxidation decreased again, the N^{1-} species were located at an average BE of 397.84 eV in Table 1. The intensities of the N^{1-} XPS spectra apparently decayed with the increase in the NH_3/O_2 gas mixing ratio and disappeared in the TiON-3 sample (Figure 1). The trend of the changing BE was opposite to what was observed for the N^{2-} and N^{3-} species. Nitrogen attracts electrons with difficulty when surrounded by an increased amount of oxygen, therefore, the shift of the outermost nitrogen electrons to their neighbors was affected by an increase in the amount of oxygen.

As the nitrogen ions were surrounded by many oxygen atoms, these ions were transferred from the electron acceptor to the electron donor. Positive nitrogen ions at high BEs transfer electrons to adjacent oxygen atoms more easily than to nitrogen ions due to the lower electronegativity of nitrogen atoms than oxygen atoms. The N chemical states of the positively charged nitrogen species corresponded to N–Ti–O and Ti–O–N–O (Table 2) [50], where nitrogen oxidation states may have corresponded to the higher BE components of N^{1+} , N^{2+} , and N^{3+} in the films deposited at low NH_3/O_2 gas mixture ratios.

Figure 8 shows the relative concentrations of various nitrogen bonding states in the total N_{1s} signal. With the increase in the NH_3/O_2 gas mixing ratio from 0.5 to 1.0, the relative concentrations of the N^{1-} and N^{1+} oxidation states decreased, while those of N^{3-} and N^{3+} oxidation states increased. NH_3 gas affected the nitridation of N-doped TiO_2 . Furthermore, with the increase in the NH_3/O_2 gas mixing ratio, the relative concentration of the N^{3-} species continuously increased. The N^{3-} species slightly served as an electron buffer for the remaining Ti at positive tetravalent ions, the electrons of which attracted the N^{3-} and O^{2-} species. The amount of N^{3-} was affected by the NH_3/O_2 gas mixing ratio. Moreover, at a low gas mixing ratio, the lack of attracted electrons led to an increase in the number of HBO species and positive N ions. Contrastingly, a large amount of N^{3-} at a high NH_3/O_2 gas mixture ratio reduced the BE and transmission of the film. These changes in N^{3+} and N^{3-} concentrations were similar to those observed by Yang et al. [51].

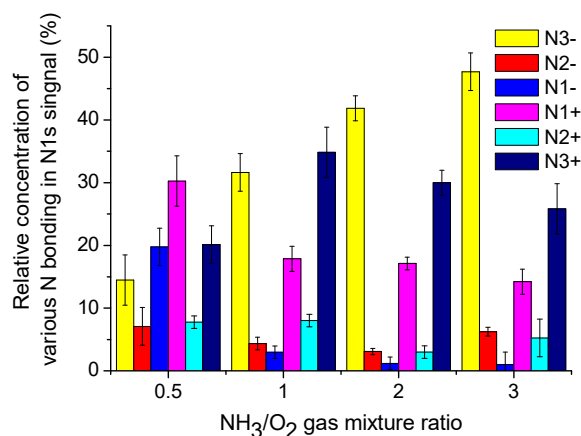


Figure 8. Changes in the N^{3-} , N^{2-} , N^{1-} , N^{1+} , N^{2+} , and N^{3+} species as functions of the NH_3/O_2 gas mixture ratios.

3.5. Optical UV-Vis Transmittance of Nitrogen-Doped TiO_2 Films

Figure 9 shows the UV-vis transmission spectra of the fused quartz substrate and as-deposited N-doped TiO_2 samples prepared by IBSD. The UV cutoff wavelengths of the N-doped TiO_2 films were considerably greater than that of the fused silica substrate. The NH_3/O_2 mixture gas apparently affected the transmission spectra of the deposited films. With the increase in the NH_3/O_2 gas mixture ratio, the transmittance decreased from 350 to 500 nm. The transmittance of samples with NH_3/O_2 ratios of 1 and 2 were higher than those of NH_3/O_2 ratios of 0.5 and 3 because the thickness of the samples with NH_3/O_2 ratios of 1 and 2 was larger than the samples with NH_3/O_2 ratios of 0.5 and 3. Regardless of the fact that the transmittances of the TiON-1 and -2 samples at 600 nm were greater than 80%, the deposited samples exhibited a red-shift due to the amount of the N-dopant, as reported by Mohamed et al. [52]. The more nitrogen and the less oxygen in the vacuum, the more O^{2-} in the

Ti–O bond was replaced by N^{3-} in the film. The $TiO_{2-x}N_x$ films noticeably absorbed the light at less than 500 nm, which was in good agreement with the theoretical and experimental results studied by Asahi et al. [2]. This observation is further discussed in the next section.

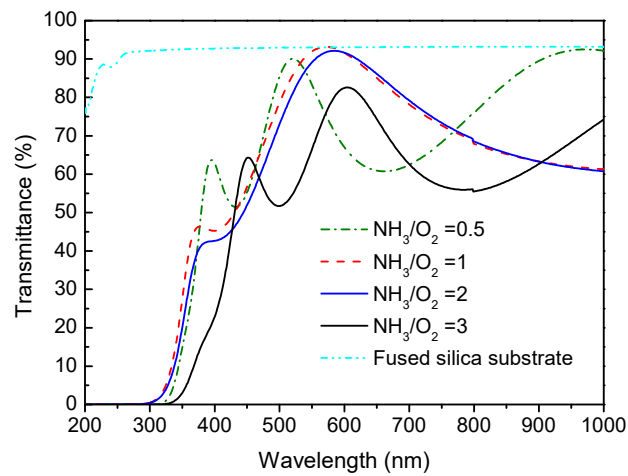


Figure 9. UV-vis transmittance of the films fabricated under various NH_3/O_2 gas ratios.

3.6. Ellipsometry of Nitrogen-Doped TiO_2 Films

Figure 10 shows the refractive indices and extinction coefficients of the films as a function of the NH_3/O_2 gas ratio, as investigated by the Tauc–Lorentz model. These films exhibited an optical index of 2.52 ± 0.02 at a wavelength of 550 nm. Moreover, the indices exhibited a large optical dispersion in a short wavelength range of 350–500 nm (Figure 10a). The $TiON_{-0.5}$, -1, and -2 samples exhibited similar trends of refractive indices as functions of the wavelength.

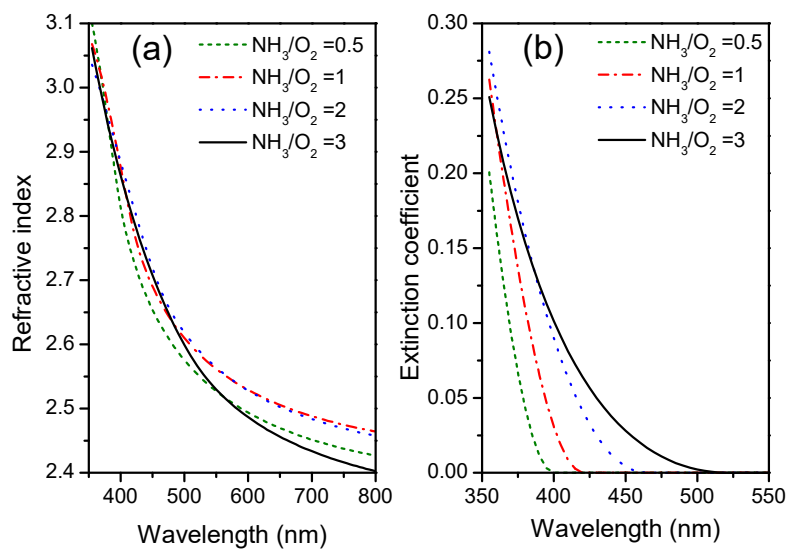


Figure 10. Refractive indices (a) and extinction coefficients (b) of the films as functions of NH_3/O_2 gas ratio and wavelength.

The films deposited using a high NH_3/O_2 gas mixing ratio also exhibited high extinction coefficients in the short wavelength range of 350–500 nm (Figure 10b). The starting absorption wavelengths, the extinction coefficients of which were zero, of $TiON_{-0.5}$, $TiON_{-1}$, $TiON_{-2}$, and $TiON_{-3}$ samples were located at ~400, 425, 450, and 500 nm, respectively, indicating that the optical bandgap energies of the films strongly depended on the NH_3/O_2 gas mixture ratio.

To increase photocatalytic reaction efficiency, it was crucial to reduce the optical bandgap of the TiO₂ film from 3.2 V. The preparation of N-doped TiO₂ with visible-light activity was considered to be a promising approach. During doping, two characteristic deep levels were located below the conduction band. The O vacancy state was active as an efficient generation–recombination center. The newly introduced N_{2p}-doped state that was generated directly above the valence band mixed with the O_{2p} valence band and contributed to the narrowing of the bandgap [53]. Asahi et al. predicted the narrowing of the bandgap using first-principle calculations [2]. In this study, when the NH₃/O₂ gas mixture ratio increased, the bandgaps evaluated by the Tauc–Lorentz model decreased from 3.1 to 2.54 eV (Figure 11). The tuning of the bandgap from 3.1 to 2.54 eV resulted from increases in complex, randomly oriented chemical N bonds and N^{3−} in the films when the NH₃/O₂ gas mixing ratio was increased, as shown in Figure 8. The bandgap narrowed in the range of 0.1 to 0.56 eV, thus, the fundamental absorption edges of the films extended to the visible-light region.

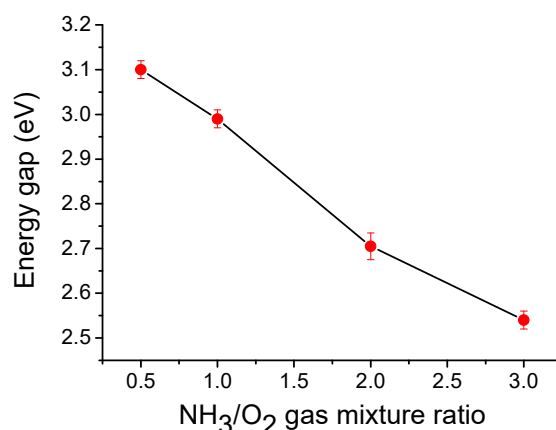


Figure 11. The decrease in the bandgap energy when the NH₃/O₂ gas mixture ratio increased.

4. Conclusions

N-doped TiO₂ films fabricated by IBSD were prepared under various NH₃/O₂ gas mixing ratios at a substrate temperature of 400 °C. All of the films were amorphous because of the complex, randomly oriented chemical bonds in the films due to the N-dopant. A significant bandgap-narrowing effect was observed on the optical bandgap down to a visible light range of 2.54 eV by fitting the data measured by ellipsometry using the Tauc–Lorentz model. Six oxidation states, N^{3−}, N^{2−}, N^{1−}, N¹⁺, N²⁺, and N³⁺ in the fitting of the N_{1s} spectra, respectively, were evaluated, even though Ti⁴⁺ was almost the only species involved in the fitting of the Ti_{2p} spectra. With the increase in the NH₃/O₂ gas mixing ratio, the bandgap narrowing reduced due to the presence of N^{3−} in the film. Various optical properties resulted from the complex N bonds in the completely oxidized N-doped TiO₂ films. This conclusion provides understanding and further development regarding the N-doped TiO₂ photocatalysts that are active under visible-light irradiation.

Author Contributions: Conceptualization, J.-C.H. and Y.-H.L.; data curation, Y.-H.L.; formal analysis, P.W.W.; funding acquisition, J.-C.H.; investigation, Y.-H.L.; methodology, J.-C.H.; project administration, J.-C.H.; resources, J.-C.H.; software, J.-C.H. and Y.-H.L.; supervision, J.-C.H.; validation, J.-C.H. and Y.-H.L.; visualization, J.-C.H.; writing—original draft preparation, P.W.W.; writing—review and editing, J.-C.H. All authors have read and agreed to the published version of the manuscript.

Funding: This research was funded by the Ministry of Science and Technology of Taiwan (Nos. MOST 105-2221-E-030-007-MY3 and MOST 106-2112-M-030-001-MY2).

Conflicts of Interest: The authors declare no conflict of interest.

References

- Zaleska, A. Doped-TiO₂: A review. *Recent Pat. Eng.* **2008**, *2*, 157–164. [[CrossRef](#)]

2. Asahi, R.; Morikawa, T.; Ohwaki, T.; Aoki, K.; Taga, Y. Visible-light photocatalysis in nitrogen-doped titanium dioxide. *Science* **2001**, *293*, 269–271. [[CrossRef](#)] [[PubMed](#)]
3. Irie, H.; Watanabe, Y.; Hashimoto, K. Nitrogen-concentration dependence on photocatalytic activity of $\text{TiO}_{2-x}\text{N}_x$ powders. *J. Phys. Chem. B* **2003**, *107*, 5483–5486. [[CrossRef](#)]
4. Zhao, Z.; Liu, Q. Mechanism of higher photocatalytic activity of anatase TiO_2 doped with nitrogen under visible-light irradiation from density functional theory calculation. *J. Phys. D Appl. Phys.* **2007**, *41*, 025105. [[CrossRef](#)]
5. Ihara, T.; Miyoshi, M.; Iriyama, Y.; Matsumoto, O.; Sugihara, S. Visible-light-active titanium oxide photocatalyst realized by an oxygen-deficient structure and by nitrogen doping. *Appl. Catal. B Environ.* **2003**, *42*, 403–409. [[CrossRef](#)]
6. Kusano, D.; Emori, M.; Sakama, H. Influence of electronic structure on visible light photocatalytic activity of nitrogen-doped TiO_2 . *RSC Adv.* **2017**, *7*, 1887–1898. [[CrossRef](#)]
7. Chen, H.; Dawson, J.A. Nature of nitrogen-doped anatase TiO_2 and the origin of its visible-light activity. *J. Phys. Chem. C* **2015**, *119*, 15890–15895. [[CrossRef](#)]
8. Livraghi, S.; Chierotti, M.R.; Giamello, E.; Magnacca, G.; Paganini, M.C.; Cappelletti, G.; Bianchi, C.L. Nitrogen-doped titanium dioxide active in photocatalytic reactions with visible light: A multi-technique characterization of differently prepared materials. *J. Phys. Chem. C* **2008**, *112*, 17244–17252. [[CrossRef](#)]
9. Sakthivel, S.; Kisch, H. Photocatalytic and photoelectrochemical properties of nitrogen-doped titanium dioxide. *Chem. Phys. Chem.* **2003**, *4*, 487–490. [[CrossRef](#)]
10. Bouhadoun, S.; Guillard, C.; Sorgues, S.; Hérisson, A.; Colbeau-Justin, C.; Dapozze, F.; Habert, A.; Mauri, V.; Herlin-Boime, N. Laser synthesized TiO_2 -based nanoparticles and their efficiency in the photocatalytic degradation of linear carboxylic acids. *Sci. Technol. Adv. Mater.* **2017**, *18*, 805–815. [[CrossRef](#)]
11. Youssef, L.; Leoga, A.J.K.; Roualdes, S.; Bassil, J.; Zakhour, M.; Rouessac, V.; Ayrat, A.; Nakhl, M. Optimization of N-doped TiO_2 multifunctional thin layers by low frequency PECVD process. *J. Eur. Ceram. Soc.* **2017**, *37*, 5289–5303. [[CrossRef](#)]
12. Wang, J.; Tafen, D.N.; Lewis, J.P.; Hong, Z.; Manivannan, A.; Zhi, M.; Li, M.; Wu, N. Origin of photocatalytic activity of nitrogen-doped TiO_2 nanobelts. *J. Am. Chem. Soc.* **2009**, *131*, 12290–12297. [[CrossRef](#)] [[PubMed](#)]
13. Miyauchi, M.; Ikezawa, A.; Tobimatsu, H.; Irie, H.; Hashimoto, K. Zeta potential and photocatalytic activity of nitrogen doped TiO_2 thin films. *Phys. Chem. Chem. Phys.* **2004**, *6*, 865–870. [[CrossRef](#)]
14. Kerr, J.A. A ready-reference book of chemical and physical data. In *CRC Handbook of Chemistry and Physics*, 1st ed.; Lide, D.R., Ed.; CRC Press: Florida, FL, USA, 2000.
15. Lee, C.C.; Hsu, J.C.; Wong, D.H. The characteristics of some metallic oxides prepared in high vacuum by ion beam sputtering. *Appl. Surf. Sci.* **2001**, *171*, 151–156. [[CrossRef](#)]
16. Jellison, G.E., Jr.; Modine, F.A. Parameterization of the optical functions of amorphous materials in the interband region. *Appl. Phys. Lett.* **1996**, *69*, 371–373. [[CrossRef](#)]
17. Tauc, J.; Grigorovici, R.; Vancu, A. Optical properties and electronic structure of amorphous germanium. *Phys. Status Solidi B* **1966**, *15*, 627–637. [[CrossRef](#)]
18. Forouhi, A.R.; Bloomer, I. Optical dispersion model relations for amorphous semiconductors and amorphous dielectrics. *Phys. Rev. B* **1986**, *34*, 7018–7026. [[CrossRef](#)]
19. Woollam, J.A. *Guide to Using WVASE 32*; J. A. Woollam Co. Inc.: Nebraska, NE, USA, 2002.
20. Selcuk, S.; Selloni, A. Facet-dependent trapping and dynamics of excess electrons at anatase TiO_2 surfaces and aqueous interfaces. *Nat. Mater.* **2016**, *15*, 1107–1112. [[CrossRef](#)]
21. Hsu, J.C.; Lee, C.C. Single- and dual-ion-beam sputter deposition of titanium oxide films. *Appl. Opt.* **1998**, *37*, 1171–1176. [[CrossRef](#)]
22. Karunagaran, B.; Rajendra Kumar, R.T.; Mangalaraj, D.; Narayandass, S.K.; Mohan Rao, G. Influence of thermal annealing on the composition and structural parameters of DC magnetron sputtered titanium dioxide thin films. *Cryst. Res. Technol.* **2002**, *37*, 1285–1292. [[CrossRef](#)]
23. Hsu, J.C.; Wang, P.W.; Lee, C.C. X-ray photoelectron spectroscopy study of thin TiO_2 films cosputtered with Al. *Appl. Opt.* **2006**, *45*, 4303–4309. [[CrossRef](#)] [[PubMed](#)]
24. Hsu, J.C.; Lee, C.C.; Chen, H.L.; Kuo, C.C.; Wang, P.W. Investigation of thin TiO_2 films cosputtered with Si species. *Appl. Surf. Sci.* **2009**, *255*, 4852–4858. [[CrossRef](#)]
25. Lee, C.C.; Wei, D.T.; Hsu, J.C.; Shen, C.H. Influence of oxygen on some oxide films prepared by ion beam sputter deposition. *Thin Solid Films* **1996**, *290*, 88–93. [[CrossRef](#)]

26. Pore, V.J.; Okura, S.; Suemori, H. Process for Deposition of Titanium Oxynitride for Use in Integrated Circuit Fabrication. U.S. Patent No. 9,523,148, 20 December 2016.
27. De Vietro, N.; Favia, P.; Fracassi, F.; d'Agostino, R. Acid/Base Gas/Liquid adsorption properties of carbon black modified in NH_3/O_2 RF glow discharges. *Plasma Process. Polym.* **2010**, *7*, 582–587. [[CrossRef](#)]
28. Delegan, N.; Daghrir, R.; Drogui, P.; El Khakani, M.A. Bandgap tailoring of in-situ nitrogen-doped TiO_2 sputtered films intended for electrophotocatalytic applications under solar light. *J. Appl. Phys.* **2014**, *116*, 153510. [[CrossRef](#)]
29. Pai, P.G.; Chao, S.S.; Takagi, Y.; Lucovsky, G. Infrared spectroscopic study of SiO_x films produced by plasma enhanced chemical vapor deposition. *J. Vac. Sci. Technol. A* **1986**, *4*, 689–694. [[CrossRef](#)]
30. Shahzadi, P.; Muhammad, A.; Mehmood, F.; Chaudhry, M.Y. Synthesis of 3, 7-dimethyl-2, 6-octadienal acetals from citral extracted from lemon grass, cymbopogon citrates L. *J. Antivir. Antiretrovir.* **2014**, *6*, 028–031. [[CrossRef](#)]
31. Abdullah, M.F.E.; Madzrol, N.; Sandin, R.W.P. Effects of biodiesel saturation degrees on NO_x emission and FTIR spectroscopy. *J. Appl. Sci. Proc. Eng.* **2016**, *3*, 1. [[CrossRef](#)]
32. Amores, J.G.; Escribano, V.S.; Ramis, G.; Busca, G. An FT-IR study of ammonia adsorption and oxidation over anatase-supported metal oxides. *Appl. Catal. B Environ.* **1997**, *13*, 45–58. [[CrossRef](#)]
33. Hadjiivanov, K. FTIR study of CO and NH_3 co-adsorption on TiO_2 (rutile). *Appl. Surf. Sci.* **1998**, *135*, 331–338. [[CrossRef](#)]
34. Wu, Y.T.; Yu, Y.H.; Nguyen, V.H.; Wu, J.C. In-situ FTIR spectroscopic study of the mechanism of photocatalytic reduction of NO with methane over Pt/ TiO_2 photocatalysts. *Res. Chem. Intermed.* **2015**, *41*, 2153–2164. [[CrossRef](#)]
35. Wagner, C.; Riggs, W.; Davis, L.; Moulder, J.; Muilenberg, G. *Handbook of X-Ray Photoelectron Spectroscopy*; Perkin-Elmer Inc.: Massachusetts, MA, USA, 1979.
36. Yu, Y.P.; Xing, X.J.; Xu, L.M.; Wu, S.X.; Li, S.W. N-derived signals in the X-ray photoelectron spectra of N-doped anatase TiO_2 . *J. Appl. Phys.* **2009**, *105*, 123535. [[CrossRef](#)]
37. Zajac, A.T.; Radecka, M.; Zakrzewska, K.; Brudnik, A.; Kusior, E.; Bourgeois, S.; Marco de Lucas, M.C.; Imhoff, L. Structural and electrical properties of magnetron sputtered Ti(ON) thin films: The case of TiN doped in situ with oxygen. *J. Power Sources* **2009**, *194*, 93–103. [[CrossRef](#)]
38. Lahoz, R.; Espinós, J.P.; Fuente, G.F.D.; Elipe, A.R.G. “in situ” XPS studies of laser induced surface cleaning and nitridation of Ti. *Surf. Coat. Tech.* **2008**, *202*, 1486–1492. [[CrossRef](#)]
39. Panda, A.B.; Laha, P.; Harish, K.; Sarkar, B.; Chaure, S.V.; Sayyad, W.A.; Jadhav, V.S.; Kulkarni, G.R.; Sasmal, D.; Barhai, P.K.; et al. Study of bactericidal efficiency of magnetron sputtered TiO_2 films deposited at varying oxygen partial pressure. *Surf. Coat. Tech.* **2010**, *205.5*, 1611–1617. [[CrossRef](#)]
40. Jia, T.; Fu, F.; Yu, D.; Cao, J.; Sun, G. Facile synthesis and characterization of N-doped TiO_2/C nanocomposites with enhanced visible-light photocatalytic performance. *Appl. Surf. Sci.* **2018**, *430*, 438–447. [[CrossRef](#)]
41. Cheung, S.H.; Nachimuthu, P.; Joly, A.G.; Engelhard, M.H.; Bowman, M.K.; Chambers, S.A. N incorporation and electronic structure in N-doped TiO_2 (110) rutile. *Surf. Sci.* **2007**, *601*, 1754. [[CrossRef](#)]
42. Gartner, M.; Osiceanu, P.; Anastasescu, M.; Stoica, T.; Stoica, T.F.; Trapalis, C.; Todorova, N.; Lagoyannis, A. Investigation on the nitrogen doping of multilayered, porous TiO_2 thin films. *Thin Solid Films* **2008**, *516*, 8184–8189. [[CrossRef](#)]
43. Yamada, K.; Yamane, H.; Matsushima, S.; Nakamura, H.; Sonoda, T.; Miura, S.; Kumada, K. Photocatalytic activity of TiO_2 thin films doped with nitrogen using a cathodic magnetron plasma treatment. *Thin Solid Films* **2008**, *516*, 7560–7564. [[CrossRef](#)]
44. Balaceanu, M.; Braic, V.; Braic, M.; Kiss, A.; Zoita, C.N.; Vladescu, A.; Drob, P.; Vasilescu, C.; Dudu, D.; Muresanu, O. Structural, mechanical and corrosion properties of $\text{TiO}_x\text{N}_y/\text{ZrO}_x\text{N}_y$ multilayer coatings. *Surf. Coat. Technol.* **2008**, *202*, 2384–2388. [[CrossRef](#)]
45. Glaser, A.; Surnev, S.; Netzer, F.P.; Fateh, N.; Fontalvo, G.A.; Mitterer, C. Oxidation of vanadium nitride and titanium nitride coatings. *Surf. Sci.* **2007**, *601*, 1153–1159. [[CrossRef](#)]
46. Jeyachandran, Y.L.; Venkatachalam, S.; Karunakaran, B.; Narayandass, S.K.; Mangalaraj, D.; Bao, C.Y.; Zhang, C.L. Bacterial adhesion studies on titanium, titanium nitride and modified hydroxyapatite thin films. *Mater. Sci. Eng. C* **2007**, *27*, 35–41. [[CrossRef](#)]
47. Zhang, M.; Lin, G.; Dong, C.; Kim, K.H. Mechanical and optical properties of composite TiO_xN_y films prepared by pulsed bias arc ion plating. *Curr. Appl. Phys.* **2009**, *9*, S174–S178. [[CrossRef](#)]

48. Braic, M.; Balaceanu, M.; Vladescu, A.; Kiss, A.; Braic, V.; Epurescu, G.; Dinescu, G.; Moldovan, A.; Birjega, R.; Dinescu, M. Preparation and characterization of titanium oxy-nitride thin films. *Appl. Surf. Sci.* **2007**, *253*, 8210–8214. [[CrossRef](#)]
49. Chan, M.H.; Lu, F.H. Preparation of titanium oxynitride thin films by reactive sputtering using air/Ar mixtures. *Surf. Coat. Technol.* **2008**, *203*, 614–618. [[CrossRef](#)]
50. Peng, F.; Cai, L.; Huang, L.; Yu, H.; Wang, H. Preparation of nitrogen-doped titanium dioxide with visible-light photocatalytic activity using a facile hydrothermal method. *J. Phys. Chem. Solids* **2008**, *69*, 1657–1664. [[CrossRef](#)]
51. Yang, T.S.; Yang, M.C.; Shiu, C.B.; Chang, W.K.; Wong, M.S. Effect of N₂ ion flux on the photocatalysis of nitrogen-doped titanium oxide films by electron-beam evaporation. *Appl. Surf. Sci.* **2006**, *252*, 3729–3736. [[CrossRef](#)]
52. Mohamed, S.H.; Kappertz, O.; Niemeier, T.; Drese, R.; Wakkad, M.M.; Wuttig, M. Effect of heat treatment on structural, optical and mechanical properties of sputtered TiO_xN_y films. *Thin Solid Films* **2004**, *468*, 48–56. [[CrossRef](#)]
53. Nakano, Y.; Morikawa, T.; Ohwaki, T.; Taga, Y. Deep-level optical spectroscopy investigation of N-doped TiO₂ films. *Appl. Phys. Lett.* **2005**, *86*, 132104. [[CrossRef](#)]



© 2020 by the authors. Licensee MDPI, Basel, Switzerland. This article is an open access article distributed under the terms and conditions of the Creative Commons Attribution (CC BY) license (<http://creativecommons.org/licenses/by/4.0/>).